# Cost-Effective and Green Additives of Pozzolanic Material Derived from The Waste of Alum Sludge for Successful Replacement of Portland Cement

**O. A. Mohamed**
Beni-Suef University
**A. A. Farghali**
Beni-Suef University
**Ashraf K Eessaa**
Electronics Research Institute
**A. M El-Shamy** ( am.elshamy@nrc.sci.eg )
National Research Centre

**Article**

**Keywords:** Alum Sludge, Morphological Characterization, CuFe2O4, Firing Stability, Compressive Strength, Water Absorption

**Posted Date:** August 4th, 2022

**DOI:** https://doi.org/10.21203/rs.3.rs-1896760/v1

# Abstract

The primary purpose of this investigation was to find out whether it would be feasible to successfully replace Ordinary Portland Cement (OPC) with 5, 10, or 15 mass % of activated alum sludge waste (AAS) as a pozzolanic material. This was the overarching question that guided the research that was conducted. A study into the use of low-cost nanocomposites to increase the physical, mechanical, and stability against the fire of OPC–AAS-hardened composites was carried out. The goal of this inquiry was to explore the utilization of low-cost nanocomposite. Producing $CuFe_2O_4$ spinel nanoparticles with an average particle size of less than 50 nm was doable. The introduction of $CuFe_2O_4$ spinel into a variety of OPC–AAS-hardened composites improve both the physicomechanical characteristics of the composites at nearly typical curing ages as well as the resistance of the composites to the effects of fire. Techniques such as TGA/DTG and XRD were utilized to provide evidence that synthesized $CuFe_2O_4$ spinel had favorable properties. These approaches revealed the presence of a range of hydration yields, such as CSHs, CASHs, CFSHs, and CuSHs, which improve the overall physicomechanical parameters as well as the thermal stability of a wide variety of OPC–AAS-hardened composites. The composite material that is composed of (90 % OPC, 10 % AAS waste, and 2 % $CuFe_2O_4$ offer several advantages, both financially and ecologically.


# 1. Introduction

As a result of the fact that it is regarded as a hazardous waste, alum sludge (AS), which is a by-product of water treatment plants, is unable to be disposed of in a landfill in a typical manner. Instead, the material must be transported to a specialized facility that is built for the express purpose of dealing with hazardous waste [1–3]. It is essential to dispose of solid wastes, particularly alum sludge (AS), as quickly as is practically practicable to reduce the number of potential threats that may be posed to the environment [4]. However, processed alum sludge, which is sometimes referred to as TAS, contains significant quantities of silica dioxide and aluminum oxide, which are the primary components of a cement [5].

As a result of this, TAS is a desirable alternative to the more traditional cement. Because of their ability to react with calcium hydroxide that is formed during the hydration of Ordinary Portland Cement (OPC), researchers in the field of concrete are becoming more interested in the practicability of recycling (AS) as a pozzolanic material with Portland cement [6]. This is because AS can interact with calcium hydroxide, which is the cause of this phenomenon. Because of the high pozzolanic activity it possesses, calcined water treatment sludge (also known as WTS) has recently been the focus of a few research studies [7]. These studies have investigated the possibility of incorporating calcined WTS as additional cementitious material in cement-based products and evaluated how doing so would impact the mechanical properties of the cement [8–10].

The results of the research indicated that the incorporation of drinking water sludge ash (DWSA) into Portland cement resulted in the development of hydrates that included aluminum. Ettringite and calcium aluminate hydrates (C–A–H) are two examples of hydrates that fall into this category since both hydrates may be found in Portland cement. This assertion is supported by the existence of a robust connection between the two variables in question. In recent years, nanotechnology has seen widespread application across virtually all areas of human endeavor to produce fresh uses. The industry of building and construction is particularly good at illustrating this trend's prevalence [11]. A lot of attention is being paid to the process of incorporating nanoparticles into cement materials. The goal of this process is to inspire new types of construction materials that have high efficiency and endurance under harsh environmental conditions [12–17]. These materials can be used in a variety of applications [18].

This is something that can be done to produce new varieties of building materials that have these qualities. These components are potentially useful in a broad variety of settings due to their adaptability and versatility. Nano silica, nano iron, nano alumina, nanofibers, nano titania, and carbon nanotubes are some of the nanoparticles that are commonly utilized. Due to the characteristics that it possesses, ferrite is utilized in a broad variety of different applications as a magnetic semiconductor. In this context, "applications" refers to things like rotary transformers, noise filters, and multilayer ferrite chip components, among other things [19–21]. The electronic industry makes substantial use of ferrites, which are among the most important components of the sector's overall inventory. Recent research has been done to explore the effect that $Fe_3O_4$ spinel nanoparticles have on the durability of cementing materials. These investigations were carried out to find out more information [22].

According to the findings, the incorporation of spinel nano-$Fe_3O_4$ improves not only the thermal stability of the materials but also their resistivity against the hostile anions that are present in the matrix. This is the case even though the incorporation of spinel nano-$Fe_3O_4$ does not improve the thermal stability of the materials [23]. As was just mentioned, many studies have been carried out and published to investigate the effect that nanoparticles have on the various properties that cementitious matrices present. These studies report their findings to better understand the relationship between nanoparticles and cementitious matrices [24–26].

On the other side, there is either no research looking into the effect that $CuFe_2O_4$ spinel nanoparticles have or merely a very tiny number of studies looking into the effect that these nanoparticles have [27]. Because of this, the purpose of this research was to utilize low-cost synthesized $CuFe_2O_4$ spinel nanoparticles (CFs NPs) as an additive for boosting the mechanical properties and fire resistivity of hardened pastes made from Ordinary Portland Cement replaced by various ratios of activated alum sludge and to investigate the feasibility of the reuse of activated alum sludge for partially replacing Portland cement in construction materials, which helps in minimizing the environmental impact [28].

# 1.1. Corrosion of steel in cement

When steel is embedded in concrete, the carbonation or chlorides in the concrete are often the agents that cause the steel to corrode over time [29]. Carbonation is the process by which carbon dioxide from the air mixes with calcium from the concrete. This process is referred to by the word "carbonation" [30]. This is evidence that the pH of the concrete is decreasing, which in turn leads the steel to begin corroding [31]. Chlorides can be transferred from the concrete to the steel in a process known as chloride-induced corrosion [32]. This process can result in a significant acceleration of the pace at which corrosion occurs [33].

According to the findings of the study that has been carried out up to this point, it has been postulated that there is a certain chloride threshold level that must be achieved prior to the start of a high corrosion rate [34]. Researchers have spent decades attempting to determine this chloride threshold level; nevertheless, the findings from their investigations have been highly variable [35]. This is likely the case given the large diversity of experimental conditions that were utilized, in addition to the fact that steel and concrete of varied quality were used in the experiments [36]. The amount of moisture that is already present in the concrete is an important factor that needs to be taken into consideration [37]. It is generally accepted, thanks to the high resistivity of dry concrete, that the rate of corrosion of steel in dry concrete is low [38]. This is because of the high resistivity of dry concrete. Extremely wet concrete has a corrosion rate that is comparable to that of moderately wet concrete due to the slow rate at which oxygen travels to the surface of the steel [39].

When the moisture condition is intermediate, the rate of corrosion is high because the material has a relatively low resistivity and oxygen moves through it at a quick pace and this causes the rate of corrosion to be high. One strategy that might be utilized to cut down on the quantity of steel that corrodes in concrete is to make use of concrete that needs a significant amount of time to reach the chloride threshold level. This strategy has the potential to be applied [40]. One method that might be utilized to attain this goal is the application of a considerable layer of concrete. Other methods include employing thick forms of concretes that have a low water/cement (w/c) ratio and/or by adding additives such as micro silica that may diminish porosity, which in turn slows the chloride transit rate. Both methods are examples of alternative ways since these approaches are instances of different approaches that might be used [41].

There are currently several distinct types of cement that can be purchased from retailers. The European standard EN 197-1, which was produced by the European council for standardization in the year 2000, is used to discern between different types of cement based on how their chemical composition varies [42]. The European standard EN 206-1 (Standardization 2000), it is suggested that for concrete that is going to be exposed to the splash/spray zone of seawater, the concrete should have a water-to-cement ratio of 0.45 and a cement content of 340 kg cement by $m^3$ concrete. This is because the ratio of water to cement determines the strength of the concrete, and the cement content determines how much cement is present in the concrete [43]. Because of this, the w/c ratio is used to determine the proportion of water to cement that is present in the concrete.

# 2. Materials And Methods

## 2.1. Materials

The Blaine surface area of Ordinary Portland cement (OPC-type I) is determined to be 3495 $cm^2/g$ based on the calculations. The cement that was utilized by the participants of the study was supplied to them by the El-Sewedy cement company, which is in Al-Ain Al-Sokhna, Suez, Egypt. The processes that were utilized to purify drinking water ultimately led to the generation of a waste product referred to as water treatment plant sludge (WTPS). The water treatment plant samples (WTPS) that were acquired from the Beni-Suef facility and utilized in this investigation were obtained there. The WTPS was initially allowed to air-dry for twenty-four hours in an oven set to 105 $^oC$ before being crushed. The alum sludge used in this study went through a procedure known as thermal activation, which was a part of the research process. To do this, dried WTPS was first heated in an electric furnace at a temperature of 500 $^oC$ for two hours before being allowed to gradually drop down to room temperature [44].

## 2.2. Methods

There were several different types of OPC–AAS dry mixes that were created and includes both the components that made them up and the names that were assigned to those components. To guarantee that every dry combination was consistent, it was exposed to eight hours of mechanical mixing in a porcelain ball mill. This was done to ensure that the mixtures were perfectly even. This was done to attain complete uniformity in the environment. The incorporation of a range of different amounts in each of the varied mixtures resulted in an improvement of the pastes (CFs NPs). Following the addition of the CFs NPs, the aqueous solution that contained the superplasticizer (which contained 0.30% of SP by mass of solid) was combined with the total quantity of mixing water, and the resulting suspensions were sonicated at a temperature of 25 $^oC$ for one hour. After mixing the dry ingredients with 0.27 parts water to 1 part cement, the resultant paste was used in several different tests [45].

When the dry materials were mixed with the necessary amount of water (which, in the case of the creation of nanocomposites, contained the dispersed CFs NPs) and the mixing technique was continued for approximately four minutes, a variety of pastes were produced. Examples of each paste were fabricated with galvanized steel that had been molded into the shape of a cube, and the dimensions of these cubes were 2.25 centimeters on each side. The freshly molded pastes were kept for one day in an environment with a relative humidity that was lower than 100% to achieve the necessary level of final setting. Following that, the specimens in the form of cubes were placed in room temperature tap water for 3, 7, and 28 days, respectively. During the compressive strength test, a machine that was made in West Germany by Ton-industries was utilized; at each stage, the average value of all three cubes was recorded. According to the method that had been described in the past, the dehydration process of the broken specimens was stopped by using a stopping solvent that was created by combining methanol and acetone in a volume ratio that was equal to 1:1.

The manufactured samples were kept at temperatures between 75 and 80 $^{o}$C for three hours before being transferred to a desiccator (which contained soda-lime and $CaCl_2$) and stored there until the time came for testing. the temperatures at which the samples were kept ranged from 75 to 80 $^{o}$C [46]. To monitor the evolution of several important physical parameters, measurements of total porosity (TP), bulk density (BD), and water absorption (WA) values were obtained at regular intervals. These measurements were taken to track the values of total porosity, bulk density, and water absorption. According to the criteria established by ASTM (C140 and C150). It is necessary to use equations 1, 2, and 3, respectively, to calculate BD, TP, and WA in that sequence. The samples that were utilized for the thermal stability test were immersed in water for 28 days, dried at temperatures of 80 $^{o}$C for one day, and then subjected to firings at temperatures of 300, 600, and 800 $^{o}$C for three hours at each temperature.

There were two ways that the burnt samples were cooled: the first set of specimens were allowed to cool gradually, while the second group was cooled quickly by being submerged in tap water. Both approaches were employed. Multiple techniques were utilized to ascertain each set of cooled specimens' respective compressive strengths. To evaluate the textural characteristics and phases that were created throughout the hydration process, selected specimens were analyzed using X-ray diffraction (XRD), thermal gravimetric analysis (TGA/DTG), and scanning electron microscopy (SEM) [47].

# 2.2.1. Corrosion Test

# 2.2.1.1. Weight Loss Measurements

The rate of corrosion was determined based on the assumption that it was uniform throughout the whole surface of the coupons. Using the following formula, we were able to determine the corrosion rate in mils per year (mpy) based on the weight loss [48]:

$$CR = \frac{W}{(D \times A \times t)} \times k \quad (1)$$

where: W = weight loss in grams, k = constant (22,300), D = metal density in g/cm$^3$, A = coupon area (inch$^2$) and t = time (days)

# 3. Results And Discussion

# 3.1. Material characterization

The XRD patterns previously carried out for activated alum sludge waste changed significantly after being subjected to calcination at a temperature of 500 $^{o}$C (AAS). The XRF for the chemical oxide compositions of OPC, the mineralogical phase compositions of OPC, and the oxide composition of AAS are outlined in Fig. 1. The pozzolanic activity of activated alum sludge waste (also known as AAS) was

evaluated following the TS 25 standards by ensuring that it met the chemical and physical requirements of standards that apply to typical pozzolanic material. This was done to determine whether the waste possessed pozzolanic activity. The TS 25 standard suggests that $SiO_2 + Al_2O_3 + Fe_2O_3$ should be at least 70%, that $SO_3$ should be less than 3.0%, that Cl should be less than 0.1%, and that the XRF study of AAS highlights the capacity of employing activated alum sludge waste (AAS) as supplemental cementitious materials (SCM) with qualities equal to those of a typical active pozzolanic material. In addition, the standard suggests the fact that XRF analysis was performed on the AAS brings this point home very clearly [49].

This investigation made use of a superplasticizer (SP) that was a modified polycarboxylate-based superplasticizer (PCsp) called Sika Viscocrete 5230 L. It has a specific gravity of 1.08 g/ml and was supplied by Sika Company in El-Obour City, Egypt. The evaluation investigated the effects of using an SP. SP superplasticizer is utilized not only as an agent for dispersing the nanoparticles but also to achieve the necessary level of workability in a variety of pastes. This is accomplished by utilizing the superplasticizer's dual-functioning ability to both disperse and work with the nanoparticles. The physical properties of the SP superplasticizer are broken out in further since its color is yellow-brown liquid, the percentage of solid residue is about 39.9%, the pH is ranged from 7.51 to 7.53 and finally, its specific gravity is about 1.08 g/ml. $CuFe_2O_4$ spinel nanoparticles (CFs NPs) with a nanoparticle size of 200 nm were created following the previously described approach as follows: utilizing commercial types of reagents and beginning components to lower the economic cost.

To determine whether the mixture was homogeneous, two moles of pure fine powder ferric acetate basic ($(CH_3COO)_2$ FeOH) were thoroughly combined in a ball mill for six hours with one mole of copper (II) acetate monohydrate ($(CH_3COO)_2$ $CuH_2O$) [50]. Following that, the mixture was dried at a temperature of 150 $^oC$, and the sample was heated on a hot plate so that the acetates could be broken down more easily. To get copper ferrite nanocrystals, the sample was finally subjected to a two-hour-long heating process at a temperature of 100 $^oC$. using SEM, the CFs NPs that had been produced at a size of 200 nm were subjected to a mechanochemical degradation process, which resulted in the generation of CFs NPs that had an average particle size of less than 50 nm as seen in Fig. 2.

The material was ball milled for forty hours to achieve this result, and then it was subjected to two hours of progressive heating in a muffle furnace at temperatures ranging from 300–500 $^oC$. The CFs NPs that were obtained had a size of 50 nm and had a value of 39.1 emu/g for their saturated magnetic flux density (Bs), and 4.002 emu/g for their remnant magnetic flux density (Br), and 85.56 Oe for their high coercivity. Additionally, the CFs NPs had a value of 39.1 emu/g for their remnant magnetic flux density (Br) (Hc). The investigation revealed that it preserves a purity level of at least 99.0% throughout its operation. The characteristics and the general properties of $CuFe_2O_4$ spinel nanoparticles are studied since their crystallite size is about 49 nm, the remnant magnetic flux density is about 4.002 $B_r$ (emu/g), as well as the saturated magnetic flux density, is about 39.11 $B_s$ (emu/g), and finally, its high coercivity is

about 85.56 $H_c$ (Oe). (CFs NPs). The design and the percentage composition of the different mixtures are outlined in Fig. 3.

# 3.2. Water absorption

The results of this experiment are depicted in Fig. 4a-d, and they may be summarized in the following way the following conclusions about the water absorption capacities of Mixes A–D were obtained from this experiment. The water absorption (WA) values of all the tested composites decreased as the aging process continued. Blended composites made from Mixes B0 and C0 displayed lower WA percentages as compared to neat OPC (Mix A), while Mix D0 showed comparable or slightly higher value after 28 days.

The incorporation of CFs NPs within the OPC–AAS pastes induced the reduction in TP %, which caused declines in the water absorption value of the pastes and the results of the CS, BD, TP, and WA tests indicate that the nanocomposite with the composition 90OPC–10AAS–2CFs has the optimal composition for application and these test results were found. This is because it demonstrates the best possible physical characteristics in comparison to all the other mixes that were tested throughout most of the testing periods (86.94 Mpa for the CS test; 2.33 g/cm$^3$ for the BD test; 35.12% for the TP test; and 12.99% for the WA test after 28 days of hydration) [51].

# 3.3. Bulk density

Figures 5a–d is a graphical representation of the findings that were obtained by measuring the bulk density (g/cm$^3$) of a variety of various mixtures. The values of the bulk density (BD) during the hydration process indicated a steady increase from day one to day twenty-eight for each composite that was put through the test. These findings might be explained by the gradual stuffing of pores with accumulated hydration products over time, which allowed for the formation of a dense and thick framework. This occurred as a direct consequence of the buildup of hydration-related compounds. As can be seen in Fig. 5a, the BD values of Mixes B0 and C0 are either more than or comparable to those of the control (Mix A), however, the BD values of Mix D0 are either less than or comparable to the control (Mix A) and the results of this investigation agree with those found in the previous study (CS).

The BD values of the composites that were made from Mixes B0 and C0 increased because of the excessive amount of hydration products that were formed because of the pozzolanic reaction between calcium hydroxide that was liberated from cement clinker hydration and AAS waste. This reaction took place because of the pozzolanic reaction between calcium hydroxide that was liberated from cement clinker hydration and AAS waste. This is a consequence of the pozzolanic reaction that took transpired, which may be explained because these products are piled in most of the open spaces (pores) along with the hardened cement matrix, and the overall porosity of the hardened composites is reduced, which is a topic that will be covered in the subsequent section. At the same time, the BD values of the hardened composites are increased. In the case of the composite built from Mix D0, the number of extra hydration products generated because of the pozzolanic interaction between the available CH and AAS is lower

than it is in the case of the composite built from Mixes B0 and C0 for the parameters that were previously indicated and listed in the section on compressive strength.

Because of this, the DB values of this mix were lower than those of (Mixes B0 and C0), but they were still comparable to those of the blank (Mix A) and the most significant discovery is that the hardened nanocomposites, which contain CFs NPs, have higher bulk density values than the materials that served as controls (Mixes A, B0, C0, and D0), and that the densification effect, which is characterized by high bulk density values, increases as the concentration of CFs NPs does as well mentioned in Figs. 5b–d. This finding can be attributed, without a shadow of a doubt, to the activation effect of CFs NPs. CFs act as foreign nucleation centers, which speeds up the hydration process and promotes the formation of an extra amount of C-S-H gel [calcium silicate hydrate ($3CaO.2SiO_2.3H_2O$], CASH, CAH [calcium aluminate hydrate $3CaO.AlO_3.6H_2O$] (CuSH) [52].

# 3.4. Total porosity

These extra chemicals congregate in the pores that are accessible, which results in the formation of a structure that is denser, more compact, and with a greater BD. The results of the analysis of the total porosity of the different composites that were tested are presented graphically in Figs. 6a–d. As can be seen in Fig. 6a, the values of the TP % decreased steadily during the hydration process (which lasted anywhere from one to twenty-eight days) for all the mixes (A to D). This transformation took place as a natural consequence of the hydration process. The stacking of distinct hydrates that grew inside the accessible spaces coupled with the composite matrix is responsible for this decrease in size. Mix B0 and Mix C0 both have TP values that are lower than those of the control sample (Mix A). On the other hand, the TP values for Mix D0 are the same as those of the blank sample. This is an additional point of interest. These findings, along with the findings of the BD and CS, do correlate, and the reasoning behind this correlation may be found in the parts that were just described.

In addition, the incorporation of CFs NPs resulted in a discernible reduction in the total porosity of all the created nanocomposites in comparison to their control, and Figs. 6b–d demonstrates that this reduction in the total porosity percentage is proportional to the quantity of CFs that were mixed in. The integration of CFs NPs results in a decreased percentage of overall porosity. This may be because the CFs NPs perform the functions of both a filler and an activator [53].

# 3.5. Thermal resistivity

It was investigated what would happen if hardened composites made from OPC, OPC-AAS, and OPC-AAS-CFs were heated to higher temperatures (300, 600, and 800 $^oC$) for 28 days. Figures 7a–b is a graphical representation of the CS values that were obtained for the various composites after being exposed to fire at various temperatures for 3 hours and then being left for gradual cooling in air. These values were obtained after the composites were left for gradual cooling in the air after being removed from the fire. The following is an account of the most important findings obtained. When compared to their recorded

values after 28 days of hydration, the compressive strength values of all composites increased significantly during heating up to 300°C; however, these values decreased significantly during heating up to 600 and 800°C. The compressive strength values of all OPC–AAS composites increased significantly when compared to those of neat OPC cement (Mix A) at all testing temperatures.

The compressive strength values of all composites increased significantly when compared to those of the following is an example of one explanation that might be correct for these results and the high upgrading of the CS values after being subjected to 300°C could be attributed to the hydrothermal reaction (internal autoclaving) that takes place between the $H_2O$ vapor molecules generated from the evaporation of physically adsorbed water inside different pores along with the hardened cement matrix and the residual unreacted cement grains. This reaction takes place between the $H_2O$ vapor molecules generated from the evaporation of physically adsorbed water inside different pores along with the hardened cement. This reaction takes place between the molecules of $H_2O$ vapor that are produced because of the evaporation of water that has been physically adsorbed inside of certain pores.

The perfect dispersion of CFs NPs within the composite matrix can be attributed to the obvious improvement in the thermal stability of a variety of nanocomposites (especially Mix D3) at 300°C. This improvement can also be attributed to the composite matrix's efficiency in inducing the formation of large quantities of a variety of hydration products via its nucleation effect and activation of the internal autoclaving. Mix D3 exhibited the greatest degree of improvement in thermal stability mixture. The nanocomposite known as D3 is the one that has demonstrated the largest increase in its thermal stability. These products get lodged in the easily accessible gaps (both macropores and micropores) along with the hardened composite, which supports the creation of the hardened matrix, which possesses a high level of resistance to the damaging effects of fire. The decrease in CS values that were observed for all composites after being exposed to 600°C can be primarily attributed to the thermal degradation of nearly all fundamental products such as CSH composites after firing at 800°C can be attributed to the complete thermal degradation for all binding centers, in addition to the induction of several cracks along with the composite matrix. This was observed after the composites had been subjected to the temperature.

After exposing the composites to the temperature, this was the resultant observation was made. Figures 7a–b illustrates the change in CS values that occurred in several composites after being heated for three hours at temperatures of 300, 600, and 800 $^{o}$C and then having their temperature dropped quickly (by immersion in cold water). These composites have CS values that are, beyond a reasonable doubt, significantly lower than those of their equivalents, which were fired at the same temperatures and cooled in the air (slowly). As the firing temperature was increased from 300 to 800 $^{o}$C, it was observed that the CS of every composite material gradually decreased (Fig. 7a–b). This was the situation with every one of the composites.

The significant reduction in CS can be attributed to the formation of several cracks as well as the enlargement of the already generated crack (micro-cracks induced during the firing), both of which occurred because of the thermal shock that occurred during the rapid cooling process. Both events took

place because of the rapid cooling that took place. In addition, the fact that the micro-cracks were caused by the firing process can be credited for the substantial drop in CS that was seen because of this action. When the temperature was raised from 300 to 600 $^{o}$C, there was a discernible decline in the compressive strength of every composite that was evaluated, and this decline persisted until it reached zero $^{o}$C when the temperature was raised to 800 $^{o}$C. Despite this, the degree to which loss of strength occurs in blended samples, whether they include CFs NPs, is larger than that which happens in neat Portland cement pastes, whether they contain CFs NPs.

This is the case regardless of whether the blended samples contain CFs NPs. After a certain amount of time has passed, the percent relative compressive strength (RCS) (relative to their CS after 28 days) is displayed in Figs. 8a–b for all burned specimens. The RCS % values that were computed following firing at 300°C and 900°F are as follows: 125.16, 125.4, 125.53, and 128.79 for Mixes A–D0, respectively; 125.26, 125.31, and 125.43 for Mixes (A1–A3), respectively; 125.46, 125.58, and 125.61 for Mixes B1–B3), respectively; (Fig. 8a-b). These data make it abundantly evident that the nanocomposite material that is made up of 85% OPC, 15% AAS waste, and 2% CFs is the one that ought to be selected for use in thermal applications. The fact that this nanocomposite has the highest residual strength (the highest percent RCS) is the best conclusion from the point of view of both the economy and the environment. Figures 8a–b illustrates the percent relative compressive strengths (relative to their CS after 28d) of several different composites after they were subjected to fire and then rapidly cooled.

The RCS percent values for these composites are as follows: 95.17, 95.29, 95.79, and 91.12 for Mixes A–D0, respectively, 96.75, 97.45 and 97.62 for Mixes A1–A3, respectively, 96.77, 97.51, and 97.63 for Mixes B1–B3); respectively. After being fired at 300 $^{o}$C then rapidly cooled. As a result of these observations, the idea is that CFs have a good effect on strengthening the fire resistance of a range of OPC–AAS blended pastes, such as I and II, CAH, CASHs, AFm, Aft, CFSH, and CH, receive additional support. Finally, a noticeable drop in CS levels was observed across the board for all the samples that were analyzed [54].

# 3.6. Compressive strength

To undertake an examination of the treated specimens' ensuing mechanical qualities, the compressive strength (CS) values of the specimens were measured at various points throughout the hydration process. This was done so that the values could be compared with one another. In Figs. 9a-d, the CS values of the hardened composites that were produced by replacing OPC with 0%, 5%, 10%, and 15% of activated alum sludge waste (AAS) (respectively, Mixes A, B0, C0, and D0) are shown. These values were obtained by creating the hardened composites with Mixes A, B0, C0, and D0. These values were achieved by exchanging OPC for waste products generated during the manufacturing of activated alum. In general, the CS values exhibited a consistent pattern with a growing hydration period across the board for every one of the mixes that were put through the testing process.

This continuous increase in the strength values can be generally attributed to the hydration of different phases that are present in Portland cement clinker and the formation of hydration products, primarily in

the form of calcium silicate hydrates, calcium aluminate hydrates, alumino ferrite monosulfate hydrate, calcium aluminosilicate hydrate, and calcium ferrite trisulfate, also known as ettringite $C_6A_0$. In addition, when contrasted with the control (pure OPC) paste, the compressive strength values recorded by the pastes generated by substituting OPC with 5 and 10% of AAS (mass % (Mixes B0 and C0, respectively) recorded the highest values possible at each testing hydration time. These values were determined by comparing the values recorded by the control paste to the values recorded by the pastes generated by substituting OPC with 5 and 10% of AAS (Figs. 9a-d).

The higher strength values that were reported for these composites are linked to the presence of excessive amounts of nearly amorphous and illcrystalline CSH as the main product. This was obtained through the pozzolanic interaction between AAS waste (alumina and silica phases) and calcium hydroxide, which was obtained from the hydration of cement clinker [55]. These greater strength values are associated with the presence of an excessive quantity of almost amorphous and ill-crystalline CSH as the principal product.

This CSH is the culprit behind the higher strength values. These hydrates not only operate as binding sites between the un-hydrated grains that are still present in the system, but they also fill the pores that are present along with the matrix. The matrix is not completely hydrated. On the other hand, increasing the quantity of AAS waste to 15% (Mix D0) causes the CS values to become comparable to, or even lower than, those of blank after 28 days. This occurs because the CS values are affected by the amount of AAS waste. This is since the waste from the AAS gets diluted (Mix A) and this decrease in the CS can be attributed to the dilution effect of PC as a result of its replacement with high percentages of AAS waste, which in turn reduces the amount of $Ca(OH)_2$ liberated as a secondary hydration product from $C_3S$ and -$C_2S$ phases that required activating the AAS waste. In other words, the amount of $Ca(OH)_2$ liberated as a secondary hydration product from $C_3S$ and -$C_2S$ phases.

The substitution of PC with significant percentages of AAS waste is to blame for the diluting impact since PC has this discovery is compatible with the findings that have previously been published by many studies, and the results of the CS revealed that the optimal replacement ratio of OPC by AAS is 10%; this finding was also verified by the results of the CS. Figures 9a–d provides clarification of the influence that additions of 0.5, 1.0, and 2.0% CFs NPs have on the CS values of neat OPC pastes. The CFs NPs were added to the pastes. There is an illustration of the mixtures A1–A3, B1–B3, C1–C3, and D1–D3. When compared to the values of their references (Mixes A–D0), the addition of different dosages of CFs NPs to OPC or OPC substituted by different masses of AAS waste leads to a significant increase in the compressive strength values of the composite material (Figs. 9a–d).

This can be seen by comparing the values of the composite material to the values of their references. These findings can be attributed to the nanoparticle characteristics of CF spinel, which include a large specific surface area of 66 $m^2/g$, a nano dimension of 50 nm, and, finally, the good distribution of it along with the cement matrix. These characteristics enable it to fill the nano- and micropores existing among different hydration products, which results in a dense and compact structure with higher strength values

than those of their control samples (Mix A). Additionally, CFs nanoparticles perform the function of active nucleation centers, which has the effect of accelerating the hydration process of cement grains to produce new and increased quantities of a variety of hydrated phases.

Calcium aluminate hydrates ($C_3AH_6$), calcium aluminosilicate hydrate (Ca-(A)-SH), and calcium ferrosilicate hydrate (like ilvaite, $CaFe^{2+}$) are some examples of the hydrated phases that may be found here CFs nanoparticles since it has been shown that the enforcement impact of CFs NPs increases as the quantity of addition of these NPs increases (from 0.5 to 2%), which is represented as an increase in the CS values for all investigated mixtures. This is a general observation that can be made because of the finding that the quantity of addition of these NPs increases. This improvement can be due to the filling influence that the CFs NPs had on the cement matrix, which led to a decrease in the porosity of the material. In other words, the CFs NPs filled the pores in the cement matrix. In addition to this, the high alkalinity of the composite matrix, which had a pH of more than 12, encouraged the partial ionization of CFs NPs into $Cu^{2+}$ and ferric anion.

These ions have an interaction with $Ca(OH)_2$ in the presence of amorphous $SiO_2$, which is present in the AAS waste. This interaction results in the generation of an excessive amount of new hydrates, such as copper silicate hydrate $Cu_2Si_2O_7(OH)_4.nH_2O$ (CuSH), calcium ferrosilicate hydrate (such as ilvaite, $CaFe_2 + Fe^{3+}SiO_7O(OH)$, (CFSH), which strongly findings will be supported by the XRD analysis that was performed on a variety of different composites that were put through their paces. In conclusion, the research showed that composite material is known as Mix C3, which is comprised of 90% PC, 10% AAS, and 2% CFs NPs, could be regarded as the most advantageous option for use in applications relating to general construction.

This was why it demonstrated the highest CS values when compared to all the other nanocomposites that were tested at nearly all ages. This was the case since it was tested at almost all ages. The substitution of 90% of the OPC with 10% of the AAS contributes to the reduction of costs associated with the disposal of waste (landfill tax), the provision of an alternative use for recycled water-treated plant sludge, without making any assumptions about either its cost or its quality, and the protection of the environment through the conservation of energy and the reduction of the number of harmful gases ($CO_2$ and NOx) and other air pollutants emitted. There is no question that this composite (90 OPC–10AAS–2 CFs) provides a multitude of benefits, from the point of view of both the economy and the environment [56].

# 3.7. Morphology and textural characteristics

The SEM-photographs provided by EDX-analyses of OPC, OPC-AAS-2 CFs NPs at 7 and 28-days of curing are represented in Figs. 10 and 11, respectively. The improvement in hydration products forming escorted by microstructure compaction is a sign of the permanence of hydration with curing intervals at all hardened samples. A low compact microstructure is the mean feature of both of OPC -AAS and OPC-AAS-2 CFs microstructures at 7 days, and this is agreeing with the results of compressive strength, which

proved that a small amount of hydration products, as C-S-H, as well as a large amount of unreacted clinker grains closely can be detected. After 28-days of hydration, OPC-AAS-2 CFs exhibits microstructure compaction better than those of OPC -AAS at both 7- and 28-days, which is attributed to dense matrix composed of the excessive generation of force-giving phases (C-S-H, C-A-S-H, and C-F-S-H) [57,58].

# 3.8. Corrosion resistance for the blinded material

The accompanying Fig. 12a-d demonstrates how the hydration time it takes for cement to set may have a significant impact on the corrosion rates of mild steel. The investigation revealed that the corrosion rates have decreased over the course of time, which was supported by the obtained data. Along with the inherent properties of these combinations, in which the pH values were recorded at the neutral level, which decreased the corrosive influence of the surrounding mild steel medium, since the water content of cement will decrease with time, which will result in a reduction in the corrosion rates by diminishing the direct contact between the mild steel surface and the surrounding environment. Both factors will contribute to a reduction in the overall corrosion rates. The presence of mild steel in this medium makes it less corrosive than it otherwise would be as a result, the pace at which corrosion occurs slows down; this was proved by the gained results that were provided earlier in the discussion. It was also found that the corrosion rates in the mixtures shown in Fig. 12d are a considerable amount lower than the rates that were reported for the mixtures in Figs. 12a, b, and c correspondingly. This was one of the findings that was shown in Fig. 12d since these data give evidence that increasing the concentration of sludge in the combination has a favorable effect on more than one property, with a reduction in the rates of corrosion being the predominant advantage brought about by this combination.

# Conclusion

The effects of introducing small quantities of $CuFe_2O_4$ spinel nanoparticles to an environmentally friendly composite manufactured from OPC and AAS waste were studied to discover how they affected the material's physical, mechanical, microstructural, and degrading properties. It is good for the environment to produce composites from waste materials and rejected materials. The following paragraphs provide an overview of the most significant results from this investigation. All the experiments revealed that using OPC–AAS waste composite as an environmentally friendly building material was suitable, and the results of these testing were made public. Hardened composites (CS, TP, BD, and WA %) can benefit from up to 10% mass substitution of AAS waste for OPC; however, 15% mass substitution of AAS waste has little influence on hardened composites' physical and mechanical characteristics. $CuFe_2O_4$ spinel nanoparticles inserted into OPC pastes at a (mass %) level of up to 2 (mass %) may promote the production of hardened nanocomposites with improved physicomechanical properties and thermal stability. OPC, AAS waste, and CFs composite materials should be utilized in normal building applications according to the research. When compared to other nanocomposites, its CS values were the highest across the board, and as a result, nearly all the hydration stages had the highest values. Many advantages may be classified as either economic or environmental for the 90% OPC, 10% AAS, and two- CFs NPs composite material. An alternative use for recycled water-treated plant sludge that

does not compromise on cost or quality is provided by using 10% AAS instead of OPC, which reduces waste disposal costs (landfill tax) and protects the environment by reducing emissions of harmful gases ($CO_2$ and $NO_x$) and other air pollutants during the manufacturing process. A nanocomposite made up of 85% OPC, 15% AAS waste, and 2% CFs is thought to be the best option for construction that will be subjected to high temperatures, both economically and environmentally. Using TGA/DTG and XRD techniques, it was demonstrated that the presence of $CuFe_2O_4$ spinel NPs catalyzed the formation of high concentrations of CFSH, AFt, AFm, CASH, and CAHs. Because these NPs were found in the presence of these other compounds, this was possible. Proof of the existence of these elements was demonstrated by showing that the NPs were in the same areas. When the temperature was increased to 300°C and CFs NPs were added to the OPC–10 AAS composite, SEM photos revealed the enhanced microstructure and mechanical characteristics of the material. Hydration products such as rod crystals, etherate fibers, CASH plates, hexagonal CH sheets, and CuSH gels must be developed to meet this goal. For most hydration products and micro/micro-cracks, thermal degradation occurred when the OPC was burnt at 800 $^oC$, however, this was less severe than when the OPC was in its pristine form. The corrosion results proved that the existence of excess amount of sludge improved the corrosion resistant of mild steel of the blended materials.

# Declarations

### Competing Interests

The authors declare that there is no conflict of interest

### Conflicts of Interest

On behalf of all authors, the corresponding author states that there is no conflict of interest.

### Author Contribution

Ola A. Mohamed, A. A. Farghali, Ashraf K. Eessaa and Ashraf M. El-Shamy analyzed the data and wrote the manuscript. Ola A. Mohamed designed and supported the experiment, and Ashraf M. El-Shamyhelped perform the analysis with constructive discussions.

### Funding

This work was supported by own and did not receive any specific grant from funding agencies in the public, commercial, or not-for-profit sectors.

### Data availability

All data generated or analyzed during this study are included in this published article

# References

1. Liu Y., Zhuge Y., Chow C.W.K., Keegan A., Pham PN, Li D., Oh JA, Siddique R. The potential use of drinking water sludge ash as supplementary cementitious material in the manufacture of concrete blocks. *Conserv. Recy.* **168,** 105291 (2020).
2. Ramadan M., El-Gamal S.M.A., Selim F.A. Mechanical properties, radiation mitigation and fire resistance of OPC-recycled glass powder composites containing nanoparticles. *Build. Mater.* **251,** 118703 (2020).
3. Ramadan M., Amin M.S., Sayed M.A. Superior physicomechanical, fire resistivity, morphological characteristics and gamma radiation shielding of hardened OPC pastes incorporating $ZnFe_0O_4$ spinel nanoparticles. *Build. Mater.* **234,** 117807 (2020).
4. Selim F.A., Hashem F.S., Amin M. S. Mechanical, microstructural and acid resistance aspects of improved hardened Portland cement pastes incorporating marble dust and fine kaolinite sand. *Build. Mater.* **251,** 118992 (2020).
5. Baki V.A., Nayır S., Erdoğdu Ş., Ustabaş Ĺ. Determination of the Pozzolanic activities of trachyte and rhyolite and comparison of the test methods implemented. *J. Civ. Eng.* **18,** 1053–1066 (2020).
6. Samson V.A.F., Bernadsha S.B., Mahendiran M., Lawrence K.L., Madhavan J., Raj M.V.A., Prathap S. Impact of calcination temperature on structural, optical, and magnetic properties of spinel $CuFe_2O_4$ for enhancing photocatalytic activity. *J Mater Sci Mater Electron* **31,** 6574–6585 (2020).
7. He Z.H., Yang Y., Yuan Q., Shi J.Y., Liu B.J., Liang C.F., Du S.G. Recycling hazardous water treatment sludge in cement-based construction materials: Mechanical properties, drying shrinkage, and nano-scale characteristics. *J Clean Prod* **290,** 125832 (2021).
8. Kaur G., Pavia S. Chemically treated plastic aggregates for eco-friendly cement mortars. J *Mater Cycles Waste Manage* **23,** 1531–1543 (2021).
9. Pavesi T.B., Rohden A.B., Garcez M.R. Supporting circular economy through the use of red ceramic waste as supplementary cementitious material in structural concrete. *J Mater Cycles Waste Manage* **23,** 2278–2296 (2021).
10. Liu Y., Zhuge Y., Chow C.W.K., Keegan A., Pham P.N., Li D., Oh J.A., Siddique R. The potential use of drinking water sludge ash as supplementary cementitious material in the manufacture of concrete blocks. *Resour Conserv Recy* **168,** 105291 (2021).
11. Magnago R.F., TdeA B., de Aguiar A.C., Baungarten P., Mendonca B.A.B., Silva H.R.T., Egert P., Girotto E., Junior A.C., Parma G.O.C. Recycling glass-polishing sludge and aluminum anodizing sludge in polyurethane and cement composites: fire performance and mechanical properties. *J Mater Cycles Waste Manage* **23,** 1126–1140 (2021).
12. M. El-Shamy, Ibrahim Abdelfattah, Ola I. Elshafie, M. F. Shehata, Potential removal of organic loads from petroleum wastewater and its effect on the corrosion behavior of municipal networks, *J. Environ. Management,* **219,** 325-331 (2018). https://doi.org/10.1016/j.jenvman.2018.04.074
13. Ibrahim Abdelfattah, Wael Abdelwahab, Ashraf El-Shamy, Montmorillonitic clay as a Cost-Effective, Eco Friendly and Sustainable Adsorbent for Physicochemical Treatment of Contaminated Water, *J. Chem.* **65(2),** 687–694 (2022). DOI: 10.21608/ejchem.2021.92320.4378

14. Emad El-Kashef, A. M. El-Shamy, Ahmed Abdo, Elshafie A. M. Gad,Amr A. Gado, Effect of Magnetic Treatment of Potable Water in Looped and Dead-End Water Networks, *J. Chem.* **62(8),** 1467-1481 (2019). DOI: 10.21608/ejchem.2019.7268.1595
15. F. Shehata, S. El-Shafey, N. A. Ammar, A. M. El-Shamy, Reduction of $Cu^{+2}$ and $Ni^{+2}$ ions from wastewater using mesoporous adsorbent: effect of treated wastewater on corrosion behavior of steel pipelines, *Egypt. J. Chem.* **62(9),** 1587-1602 (2019). DOI: 10.21608/ejchem.2019.7967.1627
16. M. El-Shamy, Hala K. Farag, W. M. Saad, Comparative Study of Removal of Heavy Metals from Industrial Wastewater Using Clay and Activated Carbon in Batch and Continuous Flow Systems, *Egyptian Journal of Chemistry* **60(6),** 1165-1175 (2017). DOI: 10.21608/ejchem.2017.1606.1128
17. G. Ateya, F. M. Alkharafi, A. M. El-Shamy, A. Y. Saad, R. M. Abdalla, Electrochemical desulphurization of geothermal fluids under high temperature and pressure, *J. Appl. Electrochem.* **39,** 383-389 (2009). https://DOI.org/10.1007/s10800-008-9683-3
18. Arulrajah, A., Mohammadinia, A., Maghool, F., Horpibulsuk, S. Tyre derived aggregates and waste rock blends: Resilient moduli characteristics. *Build. Mater.* **201,** 207–217 (2019).
19. Silvestro, L., Gleize, P. J. P. Effect of carbon nanotubes on compressive, flexural, and tensile strengths of Portland cement-based materials: A systematic literature review. *Build. Mater.* **264,** 120237 (2020).
20. Jing, G. *et al.* From graphene oxide to reduced graphene oxide: Enhanced hydration and compressive strength of cement composites. *Build. Mater.* **248,** 118699 (2020).
21. Rocha, V. V., Ludvig, P., Trindade, A. C. C. & de Andrade Silva, F. The influence of carbon nanotubes on the fracture energy, flexural and tensile behavior of cement-based composites. *Build. Mater.* **209,** 1–8 (2019).
22. Konsta-Gdoutos, M. S., Danoglidis, P. A. & Shah, S. P. High modulus concrete: Effects of low carbon nanotube and nanofiber additions. *Appl. Fract. Mech.* **103,** 102295 (2019).
23. Birenboim, M. *et al.* Reinforcement and workability aspects of graphene-oxide-reinforced cement nanocomposites. *B Eng.* **161,** 68–76 (2019).
24. K. Farag, A. M. El-Shamy, E. M. Sherif, S. Z. El Abedin, Sonochemical Synthesis of Nanostructured ZnO/Ag Composites in an Ionic Liquid, *Zeitschrift für Physikalische Chemie,* **230(12),** 1733-1744 (2016). https://doi.org/10.1515/zpch-2016-0777
25. Ashraf K. Essa, A. M. El-Shamy and Y. Reda. Fabrication of Commercial Nano porous Alumina by Low Voltage Anodizing, *J. Chem.* **61(1),** 175-185 (2018). DOI: 10.21608/ejchem.2017.2189.1175
26. Qureshi, T. S. & Panesar, D. K. Impact of graphene oxide and highly reduced graphene oxide on cement-based composites. *Build. Mater.* **206,** 71–83 (2019).
27. Sukmak, P.; Sukmak, G.; Horpibulsuk, S.; Setkit, M.; Kassawat, S.; Arulrajah, A. Palm oil fuel ash-soft soil geopolymer for subgrade applications: Strength and microstructural evaluation. *Road Mater. Pavement Des.* **20,** 110–131 (2019).
28. Dahal, B.K., Zheng, J.J., Zhang, R.J., Song, D.B. Enhancing the mechanical properties of marine clay using cement solidification. *Georesour. Geotechnol.* **37,** 755–764 (2019).

29. Elshafie A. Gad, Ashraf M. El-Shamy, Mechanism of Corrosion and Microbial Corrosion of 1,3-Dibutyl Thiourea Using the Quantum Chemical Calculations, *Journal of Bio- and Tribo-Corrosion,* **8,** 71 (2022). https://doi.org/10.1007/s40735-022-00669-x
30. Amal M. Abdel-Karim, Ashraf M. El-Shamy, Y. Reda, Corrosion and Stress Corrosion Resistance of Al Zn Alloy 7075 by Nano-Polymeric Coatings, *Journal of Bio- and Tribo-Corrosion* **8,** 57 (2022). https://doi.org/10.1007/s40735-022-00656-2
31. Amal M. Abd Elkarim, A. M. El-Shamy, Mohamed M. Megahed, Atef Evaluation the Inhibition Efficiency of a New Inhibitor on Leaded Bronze Statues from Yemen, *ARCTIC Journal,* **71(1),** 2-33 (2018).
32. M. Megahed, M. Youssif, A. M. El-Shamy, Selective Formula as A Corrosion Inhibitor to Protect the Surfaces of Antiquities Made of Leather-Composite Brass Alloy, *Egypt. J. Chem.* **63(12),** 5269-5287 (2020). DOI: 10.21608/ejchem.2020.41575.2841
33. M. Megahed, M. M. Abdel Bar, E. S. M. Abouelez, A. M. El-Shamy, Polyamide Coating as a Potential Protective Layer Against Corrosion of Iron Artifacts, *Egypt. J. Chem.* **64(10),** 5693–5702 (2021). DOI: 10.21608/ejchem.2021.70550.3555
34. M. El-Shamy, M. M. Abdel Bar, Ionic Liquid as Water Soluble and Potential Inhibitor for Corrosion and Microbial Corrosion for Iron Artifacts, *Egypt. J. Chem.* **64(4),** 1867-876 (2021). DOI: 10.21608/ejchem.2021.43786.2887
35. Reda, A. M. El-Shamy, Ashraf K. Eessaa, Effect of hydrogen embrittlement on the microstructures of electroplated steel alloy 4130, *Ain Shams Engineering Journal* **9(4),** 2973-2982 (2018). https://doi.org/10.1016/j.asej.2018.08.004
36. M. Zohdy, R. M. El-Sherif, S. Ramkumar, A. M. El-Shamy, Quantum and electrochemical studies of the hydrogen evolution findings in corrosion reactions of mild steel in acidic medium, *Upstream Oil and Gas Technology* **6,** 100025 (2021). https://doi.org/10.1016/j.upstre.2020.100025
37. M. Zohdy, R. M. El-Sherif, A. M. El-Shamy, Corrosion and Passivation Behaviors of Tin in Aqueous Solutions of Different pH, *Journal of Bio- and Tribo-Corrosion* **7(2),** 1-7 (2021). https://doi.org/10.1007/s40735-021-00515-6
38. Reda, K. M. Zohdy, A. K. Eessaa, A. M. El-Shamy, Effect of plating materials on the corrosion properties of steel alloy 4130, *Egypt. J. Chem.* **63(2),** 579-597 (2020). DOI: 10.21608/ejchem.2019.11023.1706
39. A. Abbas, K. Zakaria, A. M. El-Shamy, S. Z. El Abedin, Utilization of 1-butylpyrrolidinium Chloride Ionic Liquid as an Eco-friendly Corrosion Inhibitor and Biocide for Oilfield Equipment: Combined Weight Loss, Electrochemical and SEM Studies. *Z. Phys. Chem.* **235(4),** 377-406 (2019). https://doi.org/10.1515/zpch-2019-1517
40. M. El-Shamy, M. A. El-Hadek, A. E. Nassef, R. A. El-Bindary, Box-Behnken design to enhance the corrosion resistance of high strength steel alloy in 3.5 wt.% NaCl solution, *Mor. J. Chem.* **8(4),** 788-800 (2020). https://doi.org/10.48317/IMIST.PRSM/morjchem-v8i4.21594

41. M. El-Shamy, A Review on: Biocidal Activity of Some Chemical Structures and Their Role in Mitigation of Microbial Corrosion, *Egypt. J. Chem.* **63(12),** 5251-5267 (2020). DOI: 10.21608/ejchem.2020.32160.2683
42. Samar M. Mouneir, Ali M. El-Hagrassi, Ashraf M. El-Shamy. A Review on the Chemical Compositions of Natural Products and Their Role in Setting Current Trends and Future Goals *J. Chem.* **65(5),** 491-506 (2022). DOI: 10.21608/ejchem.2021.95577.4486
43. Amal M. Abdel-Karim, Ashraf M. El-Shamy, A Review on Green Corrosion Inhibitors for Protection of Archeological Metal Artifacts, *Journal of Bio- and Tribo-Corrosion* **8,** 35 (2022). https://doi.org/10.1007/s40735-022-00636-6
44. Kianimehr, M., Shourijeh, P.T., Binesh, S.M., Mohammadinia, A., Arulrajah, A. Utilization of recycled concrete aggregates for light-stabilization of clay soils. *Build. Mater.* **227,** 116792 (2019).
45. Naeini, M., Mohammadinia, A., Arulrajah, A., Horpibulsuk, S., Leong, M. Stiffness, and strength characteristics of demolition waste, glass, and plastics in railway capping layers. *Soils Found.* **59,** 2238–2253 (2019).
46. Huseien, G.F., Sam, A.R.M., Shah, K.W., Budiea, A., Mirza, J. Utilizing spend garnets as sand replacement in alkali-activated mortars containing fly ash and GBFS. *Build. Mater.* **225,** 132–145 (2019).
47. Sani, N.M., Mohamed, A., Khalid, N.H.A., Nor, H.M., Hainin, M.R., Giwangkara, G.G., Hassan, N.A., Kamarudin, N.A.S., Mashros, N. Improvement of CBR value in soil subgrade using garnet waste. *IOP Conf. Ser. Mater. Sci. Eng.* **527,** 012060 (2019).
48. M. El-Shamy, M. F. Shehata, H. I. M. Metwally, A. Melegy, Corrosion and Corrosion Inhibition of Steel Pipelines in Montmorilonitic Soil Filling Material, *Silicon,* **10(6),** 2809-2815 (2017). https://doi.org/10.1007/s12633-018-9821-4
49. A. Mohamed, S. M. A. El-Gamal, A. A. Farghali, Utilization of alum sludge waste for production of eco-friendly blended cement, *Journal of Material Cycles and Waste Management* **24,** 949–970 (2022). https://doi.org/10.1007/s10163-022-01369-x
50. Yaowarat, T., Horpibulsuk, S., Arulrajah, A., Maghool, F., Mirzababaei, M., Safuan, A.A., Chinkulkijniwat, A.R. Cement stabilisation of recycled concrete aggregate modified with polyvinyl alcohol. *J. Pavement Eng.* 1–9 (2020).
51. Standard Test Methods for Laboratory Determination of Water (Moisture) Content of Soil and Rock by Mass; ASTM International: West Conshohocken, PA, USA, (2019).
52. Kunchariyakun, K., Sukmak, P. Utilization of garnet residue in radiation shielding cement mortar. *Build. Mater.* **262,** 120122 (2020).
53. Soltani, A., Taheri, A., Deng, A., O'Kelly, B.C. Improved geotechnical behavior of an expansive soil amended with tire-derived aggregates having different gradations. *Minerals* **10,** 923 (2020).
54. Olson, D.W. Garnet, industrial. In Minerals Yearbook Metals and Minerals; Government of India: Nagpur, India, 1 (2021).

55. Horpibulsuk, S., Rachan, R., Chinkulkijiwat, A., Raksachon, Y., Suddeepong, A. Analysis of strength development in cement stabilized silty clay from microstructural considerations. *Build. Mater.* **24,** 2011–2021 (2010).
56. The comptroller General's Department. Cost of Construction Materials and Labor Costs 2021; The Comptroller General's Department: Bangkok, Thailand, (2021).
57. Reda, H. M.Yehia, A. M.El-Shamy, Microstructural and mechanical properties of Al-Zn alloy 7075 during RRA and triple aging, *Egyptian Journal of Petroleum* **31,** 9–13 (2022). https://doi.org/10.1016/j.ejpe.2021.12.001
58. Mohamed A. Abbas, Amr S. Ismail, K. Zakaria, A. M. El-Shamy, S. Zein El Abedin. Adsorption, thermodynamic, and quantum chemical investigations of an ionic liquid that inhibits corrosion of carbon steel in chloride solutions, *Scientific Reports* **12,** 12536 (2022). https://doi.org/10.1038/s41598-022-16755-6

# Figures

### Figure 1

Chemical compositions of OPC, (a) oxide composition of sludge, and (b) mineralogical phase compositions of OPC (mass %).

### Figure 2

SEM Image showing the nanoparticles of $CuFe_2O_4$

### Figure 3

The percentage composition of the different mixtures and their designations.

### Figure 4

Effect of hydration time on the percentages of water absorption at different cement composites

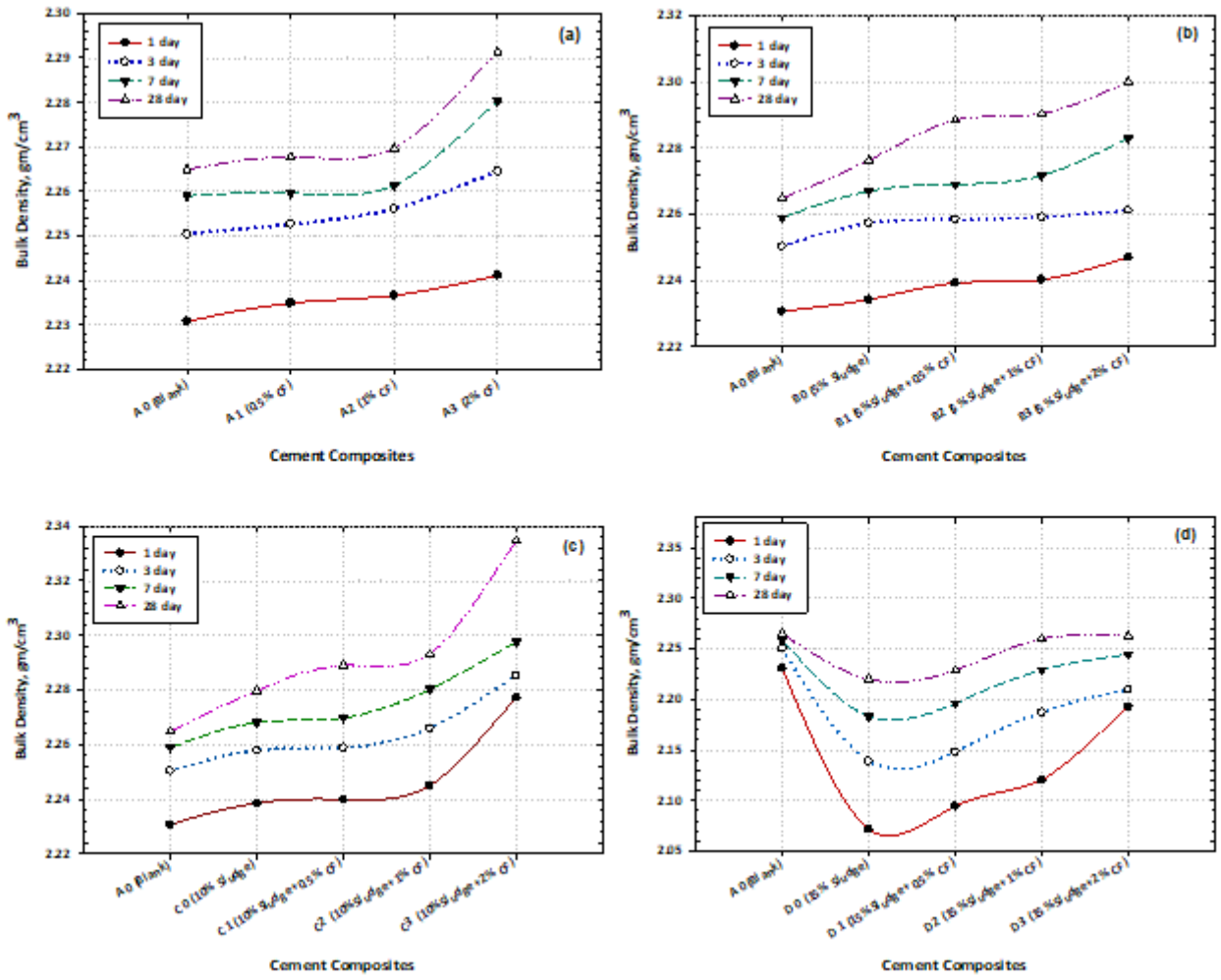


## Figure 5

Effect of hydration time on the values of bulk density at different cement composites

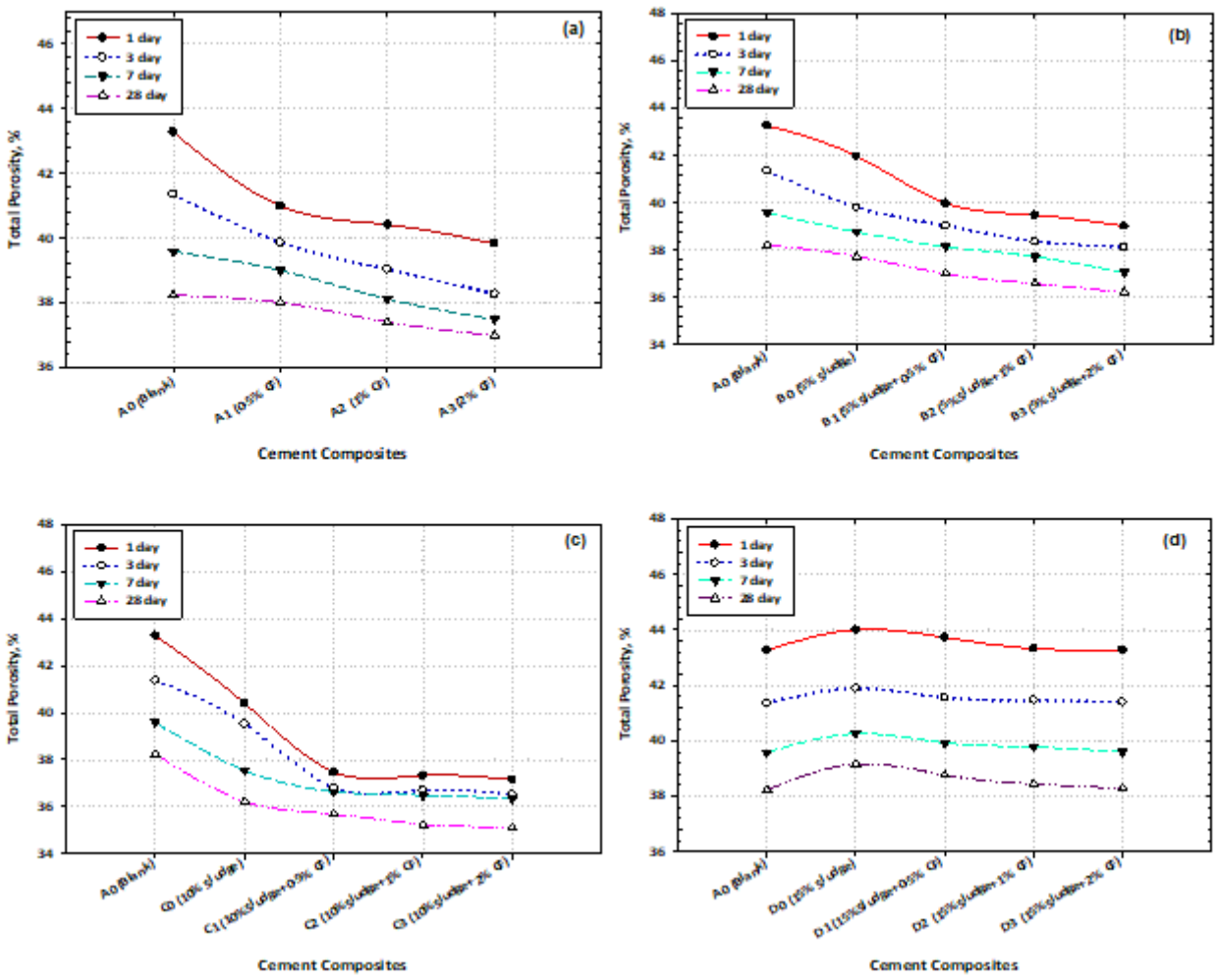


## Figure 6

Effect of hydration time on the percentages of total porosity at different cement composites

## Figure 7

Variation consequence of fired cement composites on the values of Compressive strength after (a) slow and (b) suddenly cooling

## Figure 8

Variation consequence of fired cement composites on the values of the residual compressive strength after (a) slow and (b) suddenly cooling

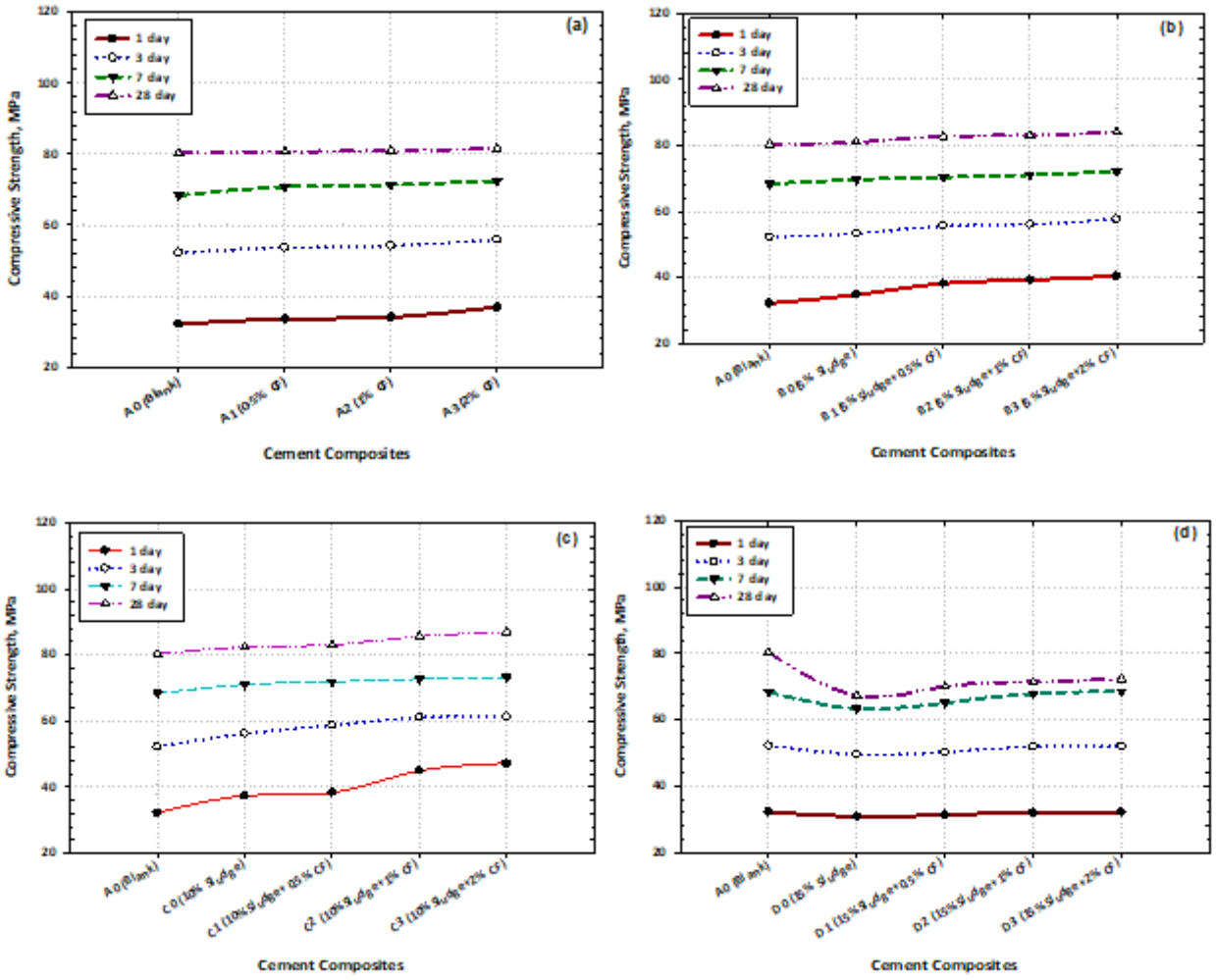


## Figure 9

Effect of hydration time on the values of compressive strength at different cement composites

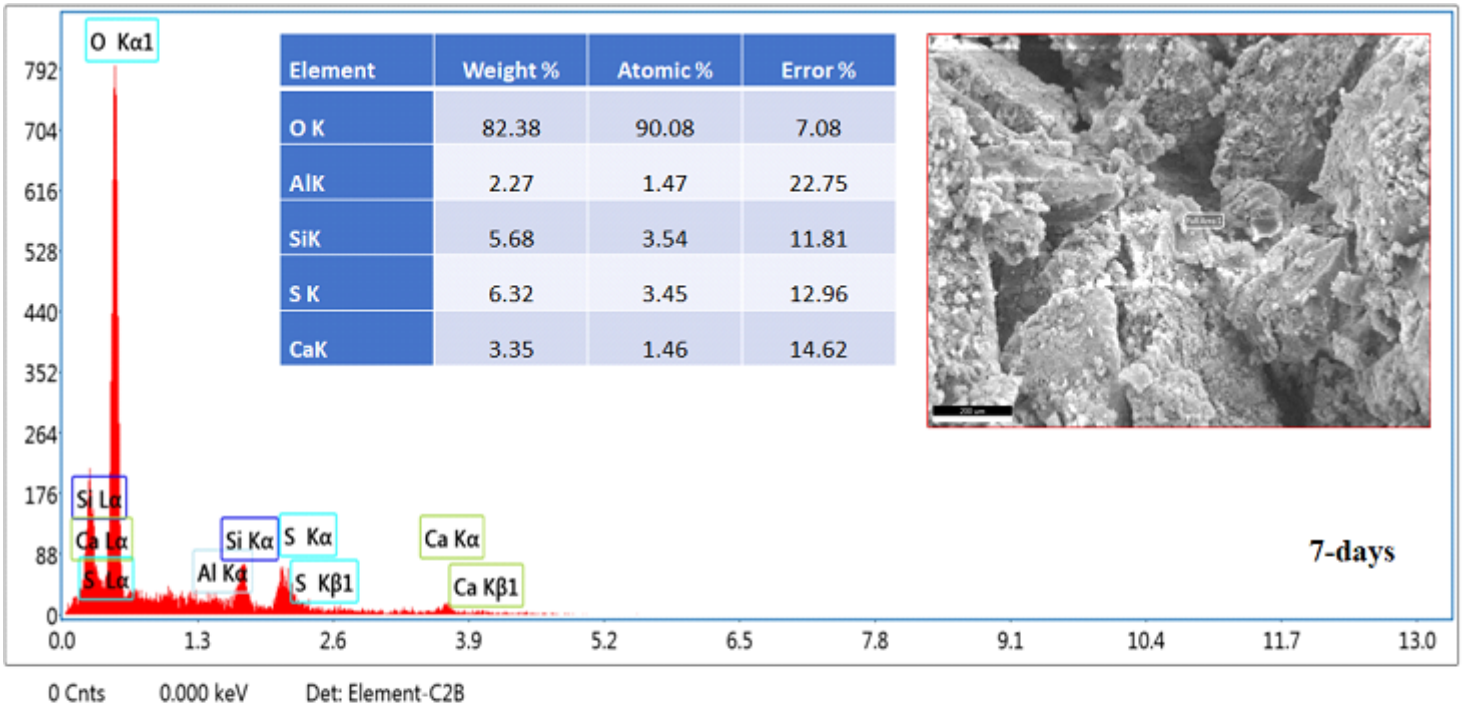


| Element | Weight % | Atomic % | Error % |
|---|---|---|---|
| O K | 82.38 | 90.08 | 7.08 |
| AlK | 2.27 | 1.47 | 22.75 |
| SiK | 5.68 | 3.54 | 11.81 |
| S K | 6.32 | 3.45 | 12.96 |
| CaK | 3.35 | 1.46 | 14.62 |

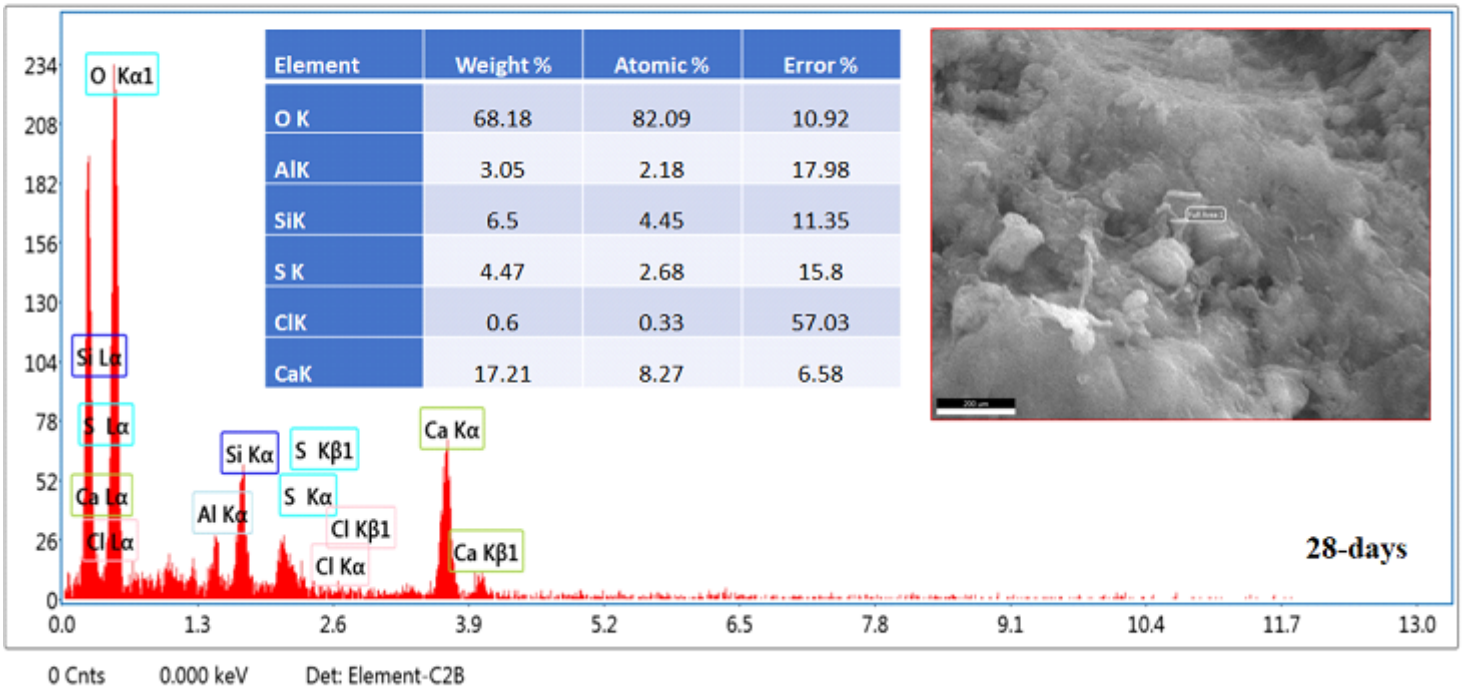


| Element | Weight % | Atomic % | Error % |
|---|---|---|---|
| O K | 68.18 | 82.09 | 10.92 |
| AlK | 3.05 | 2.18 | 17.98 |
| SiK | 6.5 | 4.45 | 11.35 |
| S K | 4.47 | 2.68 | 15.8 |
| ClK | 0.6 | 0.33 | 57.03 |
| CaK | 17.21 | 8.27 | 6.58 |

## Figure 10

SEM/EDX photographs of OPC at 7-and 28-days

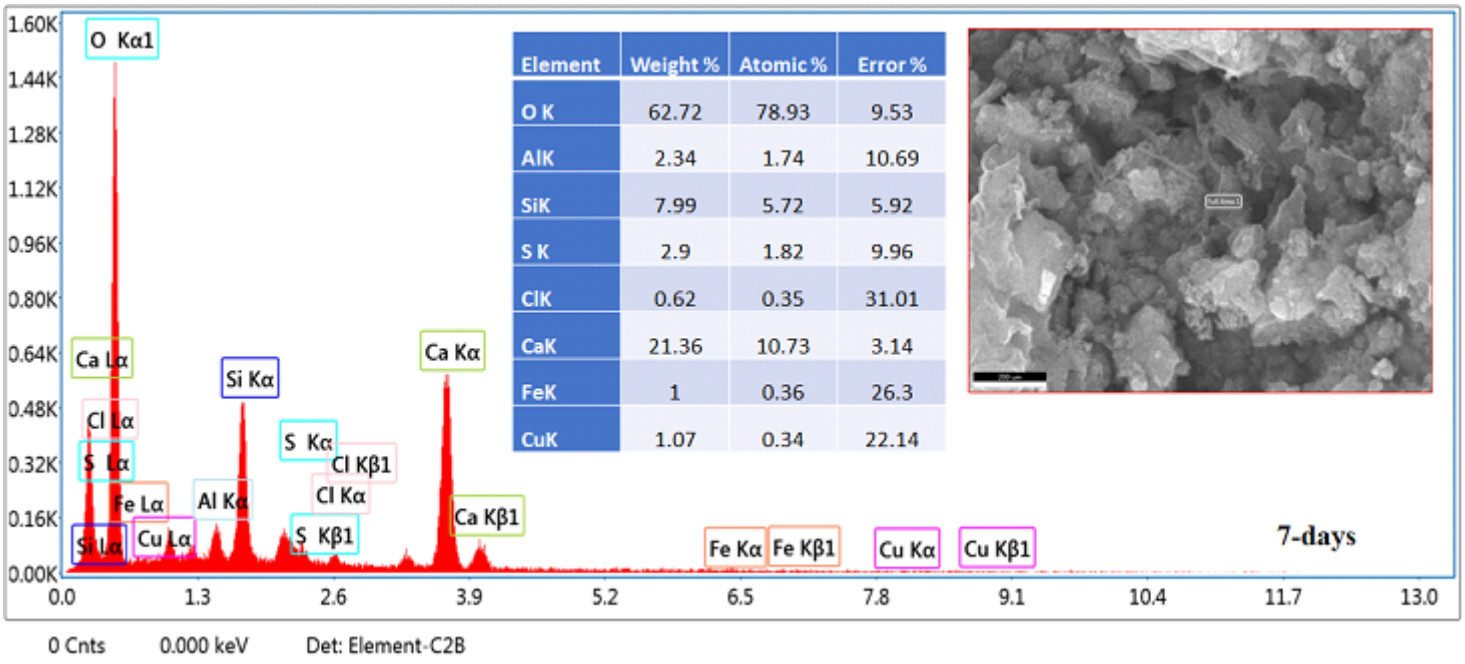


| Element | Weight % | Atomic % | Error % |
|---|---|---|---|
| O K | 62.72 | 78.93 | 9.53 |
| AlK | 2.34 | 1.74 | 10.69 |
| SiK | 7.99 | 5.72 | 5.92 |
| S K | 2.9 | 1.82 | 9.96 |
| ClK | 0.62 | 0.35 | 31.01 |
| CaK | 21.36 | 10.73 | 3.14 |
| FeK | 1 | 0.36 | 26.3 |
| CuK | 1.07 | 0.34 | 22.14 |

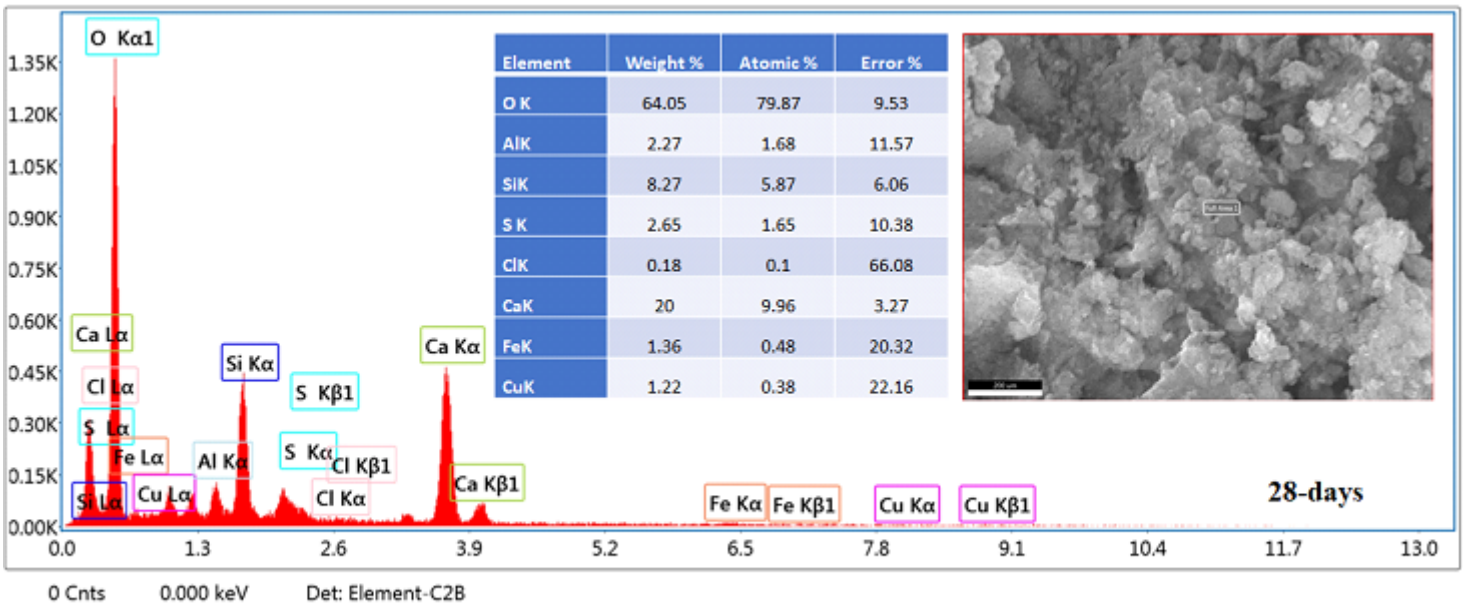


| Element | Weight % | Atomic % | Error % |
|---|---|---|---|
| O K | 64.05 | 79.87 | 9.53 |
| AlK | 2.27 | 1.68 | 11.57 |
| SiK | 8.27 | 5.87 | 6.06 |
| S K | 2.65 | 1.65 | 10.38 |
| ClK | 0.18 | 0.1 | 66.08 |
| CaK | 20 | 9.96 | 3.27 |
| FeK | 1.36 | 0.48 | 20.32 |
| CuK | 1.22 | 0.38 | 22.16 |

## Figure 11

SEM/EDX photographs of OPC-AAS-2 CFs NPs at 7-and 28-days

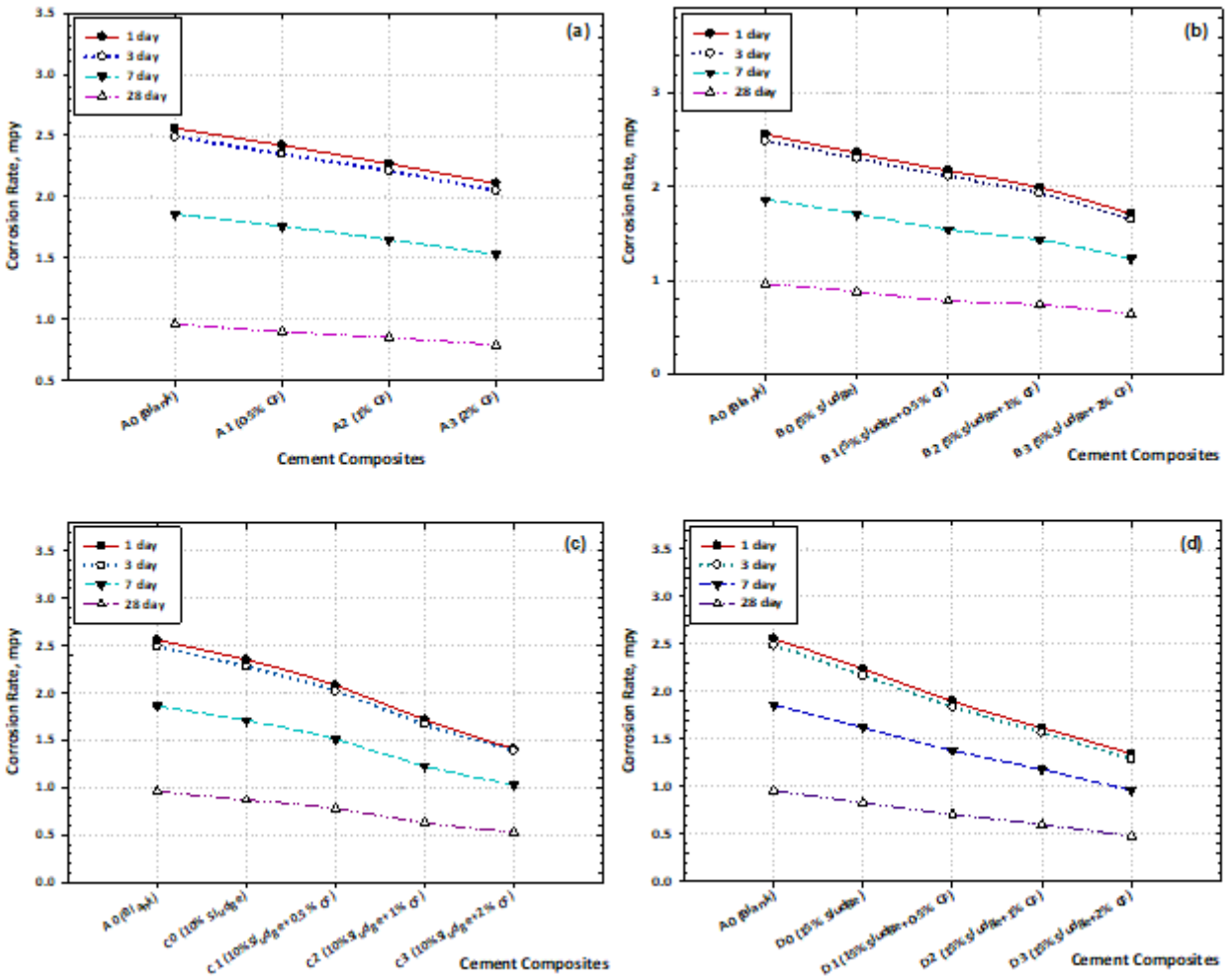


## Figure 12

Effect of hydration time on the values of corrosion rates at different cement composites